Applied Surface Science 256 (2010) 5832–5836

Contents lists available at ScienceDirect

Applied Surface Science

journal homepage: www.elsevier.com/locate/apsusc

Optical and electrical properties of Y_2O_3 thin films prepared by ion beam assisted deposition

Jian Leng, Zhinong Yu*, Yuqiong Li, Dongpu Zhang, Xiaoyi Liao, Wei Xue

School of Optoelectronics, Beijing Institute of Technology, Beijing 100081, China

ARTICLE INFO

Article history:
Received 16 November 2009
Received in revised form 10 March 2010
Accepted 10 March 2010
Available online 17 March 2010

Keywords:
Y_2O_3
Ion beam assisted deposition (IBAD)
Optical properties
Electrical properties

ABSTRACT

Y_2O_3 thin films were deposited by ion beam assisted deposition (IBAD) and the effects of fabrication parameters such as substrate temperature and ion energy on the structure, optical and electrical properties of the films were investigated. The results show that the deposited Y_2O_3 films had less optical absorption, larger refractive index, and better film crystallinity with the increase of substrate temperature or ion energy. The as-deposited Y_2O_3 films without ion-beam bombardment had larger relative dielectric constant (ε_r) and the ε_r decreased with time even over by 40%, while the ε_r of films prepared with high ion energy had less changes, only less than 3%. Also, with the increase of ion energy, the electrical breakdown strength and the figure of merit increased.

1. Introduction

Y_2O_3 films have been widely used as dielectric layers for electroluminescent devices and antireflection coatings for diamond [1–4]. In recent years, pure or doped Y_2O_3 planar optical waveguide thin films have attracted much attention due to their potential applications in optoelectronics [5,6].

Y_2O_3 films are usually deposited by electron-beam evaporation [7], pulsed laser deposition [8,9] and r.f.-magnetron sputtering [10,11]. It was reported that there were many problems while depositing Y_2O_3 films by electron-beam evaporation, for example, Y_2O_3 thin films tended to deviate from stoichiometry [12] and needed to be annealed for high quality [13]. In this paper, we report different processes to deposit Y_2O_3 films by ion beam assisted deposition (IBAD) and analyze their optical and electrical properties and find that by IBAD, high quality Y_2O_3 films could be prepared without annealing.

2. Experimental

The equipment used for Y_2O_3 film deposition was an ion beam assisted deposition system equipped with a Kaufman ion source for the supply of O_2/Ar mixture ion-beam and a turbomolecular pump. Bare k9 glass and 200 nm indium-tin-oxide (ITO) film coated k9 glass were used as substrates. The sheet resistance of the ITO film was about 12 Ω/sq, and the transmission was over 80%. Prior to deposition, the substrate surfaces were pre-cleaned using Ar^+ ion-beam bombardment for 5 min in order to further reduce impurities on the substrate surfaces. The precursor for evaporation was Y_2O_3 pills with the purity of 99.99%. During the deposition, the substrate was rotated. The distance between the substrate and the ion source and the incident ion-beam angle between the ion source and the substrate were kept at 65 cm and 40°, respectively. The chamber was evacuated to a base pressure of 2×10^{-5} Torr initially and the chamber pressure during deposition was maintained at 10^{-4} Torr. The deposition parameters are listed in Table 1.

During IBAD, ion energy (E_a) depends on accelerating voltage (U_a), the larger U_a is, the higher E_a is. The ions with higher energy can react with film particles more easily, and lead to the formation of the required chemical structure [14]. In the experiments, it was found that the properties of Y_2O_3 films varied with both substrate temperature (T_s) and ion energy (E_a). To analyze how the deposition parameters affect optical and electrical properties of Y_2O_3 thin films, an orthogonal test was designed [15,16]. The experimental schedule with different values of deposition parameters is shown in Table 2.

The growth rate and thickness of Y_2O_3 films were measured by a quartz crystal monitor. The actual thickness and refractive index were indicated by post-deposition ellipsometry measurements (VASE, J.A. Woollam Co., Inc.). The crystal structure was characterized by X-ray diffractometry (XRD) (MXP18; Mac Science Ltd.) using Cu Kα radiation, with a scanning speed of 4°/min and an incident angle of 4°. The optical transmittance was recorded by an UV/vis spectrophotometer (UV-2802S, UNICO, USA).

* Corresponding author. Tel.: +86 1 68913259x11; fax: +86 1 68912550.
E-mail addresses: znyu@bit.edu.cn, zhn_yu@yahoo.com (Z. Yu).

0169-4332/$ – see front matter © 2010 Elsevier B.V. All rights reserved.
doi:10.1016/j.apsusc.2010.03.054

Table 1
The fundamental fabrication conditions of Y_2O_3 films.

Ion energy (eV)	0–350
Ion beam current (mA)	100
Oxygen partial pressure (Torr)	2×10^{-4}
Growth rate (Å/s)	1.5
Substrate temperature (°C)	25–200
Thickness of Y_2O_3 film (nm)	400

Table 2
The experimental schedule with different values of deposition parameters.

Sample number	Substrate temperature, T_s (°C)	Ion energy, E_a (eV)
1	25	0
2	25	250
3	25	350
4	100	0
5	100	250
6	100	350
7	200	0
8	200	250
9	200	350

A measure project for the electrical properties of Y_2O_3 film is shown in Fig. 1. The Y_2O_3 films were deposited on ITO film coated k9 glass. A series of copper electrodes with the thickness of 400 nm and a radius of 1 mm were deposited on Y_2O_3 film. The current–voltage (I–V) characteristics were measured with a Keithley 2400 source/measure unit. The dielectric properties such as capacitance (C) were measured at 1 kHz and 1 V voltage by an programmable automatic RCL meter (Fluke PM 6304). The relative dielectric constant ε_r was calculated from the following equation,

$$\varepsilon_r = \frac{Cd}{\varepsilon_0 S} \quad (1)$$

where d, ε_0, S are the film thickness, the vacuum dielectric constant, and the electrode area, respectively.

3. Results and discussions

3.1. Optical properties

Due to decomposition of Y_2O_3 precursor by evaporation and loss of oxygen, it is necessary to supplement oxygen during evaporation deposition for the formation of stoichiometric Y_2O_3 film. Otherwise, the deposited Y_2O_3 film will have optical absorption. Besides the introduction of oxygen during deposition, T_s and E_a also affect the optical absorption of Y_2O_3 film. It is found that, with higher T_s or E_a, the deposited Y_2O_3 films have less optical absorption. Fig. 2 shows transmittance spectra of samples with different ion energy, and the horizontal line at 91.6% corresponds to the theoretic maximum transmittance. In the process of preparing sample 5 and sample 6, oxygen was ionized and accelerated. The oxygen ions

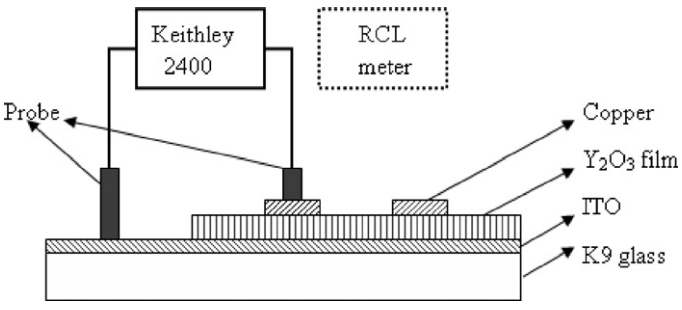

Fig. 1. Project of testing the electrical properties of Y_2O_3 films.

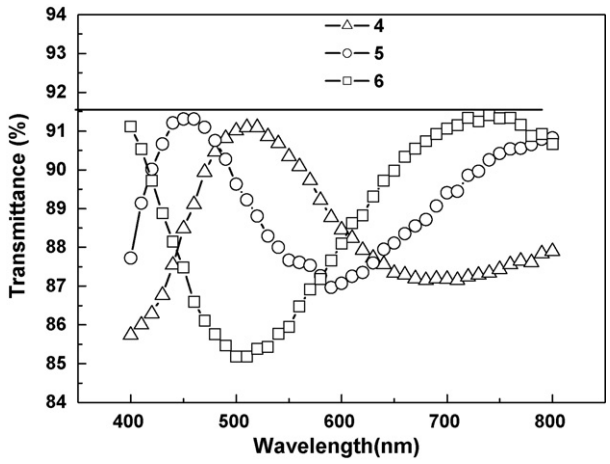

Fig. 2. Transmittance spectra of samples with different ion energy.

with high energy react with yttrium more easily, which leads to the formation of Y_2O_3 film with maximum transmittance, approximating to theoretic one (that is, without optical absorption). However, sample 4 has a little optical absorption due to insufficient oxidation of yttrium.

Although the thickness of all samples monitored by a quartz crystal oscillator was kept the same as 400 nm, it was different because of different deposition parameters, measured by spectroscopic ellipsometry. That's why samples have different transmittance peak with the change of wavelength, as shown in Fig. 2. The actual thickness of Y_2O_3 films are shown in Table 3. And there were two points to ensure the film uniformity: (1) the samples were kept spinning in the coating process; (2) the sample size (20 mm × 20 mm) was negligible comparing to the vacuum chamber (800 mm × 800 mm). The thickness of samples floats 5 nm measured by spectroscopic ellipsometry. The thickness of every series of sample encountering different tests is the same because of the same preparation condition and actual thickness is used through the analyses below.

Also, it is found that, with the increase of E_a or T_s, the refractive index (n) increases. Fig. 3 shows the refractive index (n) of samples as a function of E_a. At the same T_s of 100 °C, the refractive indexes (n) of No. 4 (0 eV), No. 5 (250 eV) and No. 6 (350 eV) at 500 nm are 1.723, 1.773, and 1.827, respectively. The refractive index reflects the film density, and this can be expressed by Drude equation [10]:

$$1 - p = \frac{n_t^2 - 1}{n_b^2 - 1} \quad (2)$$

where n_t and n_b are the refractive index of porous material and bulk material, respectively, and p is the porosity of the material. It is clear that the larger n_t is, the smaller p is, which means the material is more dense. So Fig. 3 also indicates the deposited films became dense with the increase of E_a or T_s. The formation of the dense film results from the facts that (1) the deposited Y_2O_3 molecules or clusters got higher kinetic energy and could move more freely on the surface; (2) IBAD could lead to the collapses of pores.

Table 3
Real thickness of Y_2O_3 films.

	Sample number								
	1	2	3	4	5	6	7	8	9
Actual thickness (nm)	433	369	318	452	389	337	439	380	329

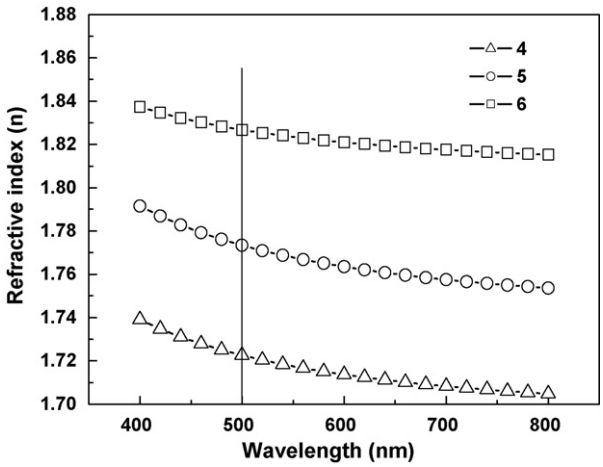

Fig. 3. Refractive index (n) of samples with different ion energy.

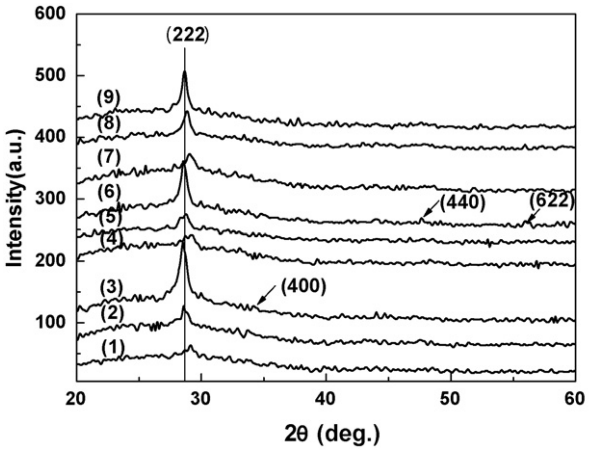

Fig. 4. XRD patterns for Y_2O_3 films deposited with different parameters.

3.2. X-ray diffraction

Fig. 4 shows the XRD results on Y_2O_3 films deposited with different parameters. We can see that all the films are polycrystalline and when T_s is below 200 °C, there is (0 0 3) peak which indicates monoclinic Y_2O_3 phase exists [17]. While T_s reaches 200 °C, the monoclinic structure disappears, and there is mainly cubic phase in the Y_2O_3 films illustrated by (2 2 2), (4 0 0), (4 4 0), (6 2 2) peaks [18]. And the diffraction intensity increases with E_a at the same T_s. So it can be concluded that the substrate temperature can change Y_2O_3 films' phase and the (2 2 2) plane is the preferential orientation during the film growth process.

Table 4 shows the data of (2 2 2) X-ray diffraction peaks of Y_2O_3 films. The peak height was obtained by calculating the peak area, and the grain size was calculated from Scherrer equation:

$$D = \frac{0.89\lambda}{\beta \cos\theta} \quad (3)$$

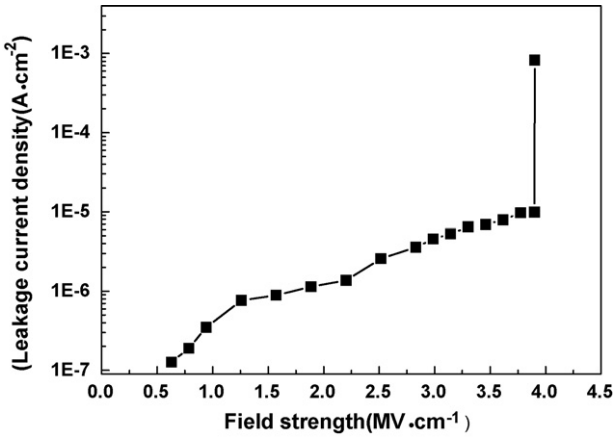

Fig. 5. I–V characteristic of sample 3.

where D is the average grain size, β the full width at half maximum(FWHM) of diffraction peak, θ is Bragg angle, and $\lambda = 1.5406$ Å (CuKα).

It can be concluded from Table 4 that, with the increase of T_s, the FWHM decreases, and the diffraction intensity and grain size increases, which could be illustrated by comparing sample 1, 4 and 7. This indicates that the crystallinity of Y_2O_3 film is improved. The energy of Y_2O_3 particles without bombardment of O_2/Ar was low if the substrate was not heated, and the lack of energy led to poor crystallinity, which illustrates that the supplement of energy by heating is in favor of grain growth and improvement of film crystallinity.

Similarly, we also see that the film crystallinity was improved with the increase of E_a, and the improvement was more obvious than that induced by heating. These features indicate that, compared with heating, the bombardment of O_2/Ar with high energy on the film surface is more effective to transfer the energy to film molecules and enhance the grain growth.

While E_a increases, film crystallinity becomes better, and grain boundaries decrease, connectivity between particles increases and grain size becomes larger, which means that film contains bigger in number and size nano-crystals illustrated by XRD data, and thus the film becomes denser. And this is consistent with the conclusion got from Drude equation in Section 3.1.

3.3. Electrical properties

Fig. 5 shows the I–V characteristic curve of No.3. The curve shape is coincident with the report of Onisawa et al. [12]. It can be seen from Fig. 5 that the current increases gradually with the increase of field strength below 3.9 MV cm^{-1}. When the field strength increases above 3.9 MV cm^{-1}, the current density reaches 8.3×10^{-4} A cm^{-2} instantly and then drops to 1.6×10^{-5} A cm^{-2}. The sudden increase of current density corresponds to the electrical breakdown of film. The breakdown electrical field E_{bd} can be calculated by the equation: $E_{bd} = U_{bd}/d$ (where U_{bd} is the electrical breakdown voltage and d is the film thickness). The other 8 samples have similar I–V characteristic curves except for different electrical breakdown voltages.

Table 4
The data of (2 2 2) X-ray diffraction peaks of Y_2O_3 films.

	Sample number								
	1	2	3	4	5	6	7	8	9
FWHM (°)	1.11	0.80	0.66	1.00	0.76	0.56	0.85	0.70	0.60
Peak height	22	34	87	23	36	69	26	39	65
Grain size (nm)	7	12	15	10	13	15	11	13	16

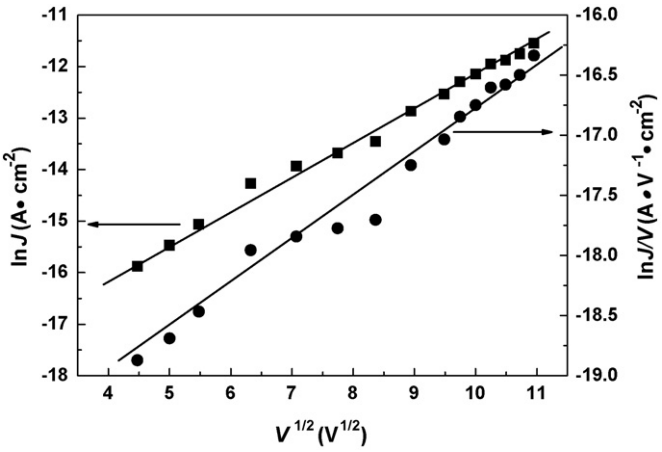

Fig. 6. Plots of ln$J$ and ln(J/V) vs. $V^{1/2}$.

In order to analyze the I–V properties in detail, the I–V properties were plotted using Schottky and Poole–Frenkel (P-F) emission models as shown in Fig. 6. Here J is current density and V is applied voltage. From Fig. 6 we can see that there is good linear relationship between ln$J$ and $V^{1/2}$ especially in high-voltage region which means Schottky emission model is applicable to the MIS structure. While the linear relationship between ln$J$/V and $V^{1/2}$ is bad indicating the non-applicability of P-F model. Thus these results indicate that Schottky emission occurs in Cu/Y_2O_3/ITO structures. And this observation is in accordance with the findings of Basak and Sen [19].

Table 5 shows the electrical properties of all the samples. ε_r, E_{bd} and Γ stand for relative dielectric constant, electrical breakdown field and figure of merit of as-deposited samples, respectively. ε_r' is relative dielectric constant of the samples measured after 3 months. It can be seen that ε_r of the sample decreases with the increase of ion energy. For example, samples 4, 5 and 6 were prepared at the same T_s of 100 °C, while sample 6 has the smallest ε_r due to the highest ion energy. This can be explained as follows.

While Y_2O_3 film is prepared by electron-beam evaporation, high-energy secondary electrons will emit from the evaporated source. These electrons will inject into the film and be captured by the defects in the film. The accumulation of charges leads to the increase of ε_r, that is, the ε_r increases with the increase of molecular dipole density N_0, which is described by Havriliak–Negami function [20]. While the films are prepared by IBAD, superfluous Ar^+ could neutralize secondary electrons from the evaporated precursor, and reduce the molecular dipole density N_0. The decrease of N_0 with the increase of ion energy leads to the decrease of ε_r, illustrated by comparing of samples 4, 5 and 6.

It can also be seen from Table 4 that ε_r', compared to ε_r, decreases by over 40% for the samples prepared at low E_a. While ε_r' of samples prepared at high E_a has less change, even less than 3%. These variations results from charge decay in the deposited films. The decay approaches can be concluded as follows: (1) the charges are drifted or spreaded by inner electric field; (2) heterogeneous charges in the surrounding environment are absorbed on the sample surface and neutralize with ones in the films; (3) nonpolar molecules such as water molecules are absorbed and increase the migration rate of the internal charges, which accelerates the decay of internal charges [21–23]. The deposited Y_2O_3 films at low E_a could capture more electrons, as mentioned above, but after a period of time, more charges will decay, leading to more obvious increase of the dielectric constant.

Table 5
Electrical properties of Y_2O_3 films.

	Sample number								
	1	2	3	4	5	6	7	8	9
ε_r	24.3	16.7	12.6	31.6	22	14.5	27.1	20.2	21.8
ε_r'	17.9	15.5	12.3	17.7	18.1	14.1	14.3	18.8	21.0
E_{bd} (MV cm^{-1})	1.82	3.17	3.9	1.48	2.65	3.24	1.64	2.26	2.88
Γ (μC cm^{-2})	3.91	4.69	4.35	4.14	5.16	4.16	3.93	4.04	5.56

Table 5 shows that E_{bd} increase obviously with the increase of E_a, regardless of substrate temperature. This can be explained by comparing samples 1, 2 and 3. Because the deposited Y_2O_3 film at low T_s and low E_a as sample 1 has porous structure, while top Cu electrode is deposited on the porous Y_2O_3 film, Cu atoms can transfer through the pores, which could reduce the distance between the upper and lower electrodes and increase the possibilities of the electrical breakdown [24,25]. But in samples 2 and 3, because of the decrease of porosity by bombardment of O_2/Ar ion with high energy as mentioned in Section 3.1, Cu atoms cannot penetrate Y_2O_3 film easily and the samples have larger field strength. So IBAD has a positive role in improving the breakdown electrical field of Y_2O_3 film.

The E_{bd} of samples placed for 3 months were also tested, and the results were almost the same as the as-deposited samples.

The figure of merit $\Gamma = \varepsilon_0\varepsilon_r E_{bd}$ is usually used to evaluate the charge storage capacity of Y_2O_3 thin film, especially when Y_2O_3 film is used in electroluminescent devices. Γ should be at least 3 times of the active layer [1] to ensure that device has a high luminous efficiency. Typically this means that the charge storage capacity should be greater than 3 μC cm^{-2} [26]. From Table 4 we can see that Γ of all the Y_2O_3 films sample is greater than 3 μC cm^{-2} and sample 9 prepared at high both T_s and E_a, has the largest figure of merit Γ = 5.56 μC cm^{-2} which is almost the same as Cranton's results prepared at high temperature.

4. Conclusion

Ion beam assisted deposition was adopted to deposit Y_2O_3 thin films with different parameters. It was found that the deposited Y_2O_3 films at higher substrate temperature or with higher ion energy had less optical absorption, larger refraction index and better film crystallinity. In the electrical characteristics, Y_2O_3 films deposited without ion-beam bombardment had large relative dielectric constant, but the constant decreased with time rapidly, even over 40%. With the increase of ion energy, the relative dielectric constant decreased and had less change with time, the electrical breakdown strength and the figure of merit increased. So IBAD has obvious advantages in preparing the dielectric films with low optical absorption as well as high electrical stability and breakdown strength.

References

[1] W.M. Cranton, D.M. Spink, R. Stevens, C. Thomas, Growth and dielectric characterization of yttrium oxide thin films deposited on Si by r.f.-magnetron sputtering, Thin Solid Films 226 (1993) 156–160.
[2] T.P. Mollart, C.J.H. Wort, C.S. Pickles, CVD diamond optical components, multispectral properties and performance at elevated temperatures, Proc. SPIE 4375 (2001) 180–198.
[3] T.P. Mollart, K.L. Lewis, C.J.H. Wort, C.S.J. Pickles, Coating technology for CVD diamond optics, Proc. SPIE 4375 (2001) 199–205.
[4] K.A. Klemm, H.S. Patterson, L.F. Johnson, M.B. Moran, Protective optical coatings for diamond infrared windows, Proc. SPIE 2286 (1994) 347–356.
[5] Y.S. Kim, W.H. Kim, Optical loss mechanism in yttria thin film waveguides, Opt. Mater. 14 (2000) 229–234.
[6] M.B. Korzenski, Ph. Lecoeur, B. Mercey, P. Camy, J.L. Doualan, Low propagation losses of an Er:Y_2O_3 planar waveguide grown by alternate-target pulsed laser deposition, Appl. Phys. Lett. 78 (2001) 1210–1212.
[7] R.N. Sharma, S.T. Lakshmikumar, A.C. Rastoqi, Electrical behavior of electron-beam-evaporated yttrium oxide thin films on silicon, Thin Solid Films 199 (1991) 1–8.

[8] S.Q. Zhang, R.F. Xiao, Yttrium oxide films prepared by pulsed laser deposition, J. Appl. Phys. 83 (1998) 3842–3848.
[9] C.W. Lin, T.Y. Cheng, L. Chang, J.Y. Juang, Chemical vapor deposition of zinc oxide thin films on Y_2O_3/Si substrates, Phys. Stat. Sol. C 4 (2004) 851–855.
[10] X.J. Wang, L.D. Zhang, J.P. Zhang, G. He, M. Liu, L.Q. Zhu, Effects of post-deposition annealing on the structure and optical properties of Y_2O_3 thin films, Mater. Lett. 62 (2008) 4235–4237.
[11] H.S. Kim, C. Park, R.K. Ko, D. Shi, J.K. Chung, H.S. Ha, Y.M. Park, K.J. Song, D.J. Youm, High rate DC-reactive sputter deposition of Y_2O_3 film on the textured metal substrate for the superconducting coated conductor, Physica C 426–431 (2005) 926–932.
[12] K. Onisawa, M. Fuyama, K. Tamura, K. Taguchi, T. Nakayama, Y.A. Ono, Dielectric properties of rf-sputtered Y_2O_3 thin films, J. Appl. Phys. 68 (1990) 719–723.
[13] A.C. Rastogi, R.N. Sharma, Structural and electrical characteristics of metal–insulator–semiconductor diodes based on Y_2O_3 dielectric thin films on silicon, J. Appl. Phys. 71 (1992) 5041–5052.
[14] Y.Q. Pan, C. Zhu, Q. Mi, J.J. Song, The optical properties of TiO_2 thin film prepared by electron beam evaporation, J. Appl. Phys. Optics 5 (2004) 53–55.
[15] Y.H. Zhao, G.Q. Liu, J.Q. Xiao, C. Dong, L.Sh. Wen, Effect of sample configuration on droplet-particles of TiN films deposited by pulse biased arc ion plating, J. Mater. Sci. Technol. 25 (2009) 681–686.
[16] K.M. Hung, C.S. Hsieh, W.D. Yang, Y.J. Sun, The preparatory optimal conditions of barium titanate thin film from a hydrothermal method at low temperature, J. Mater. Sci. 42 (2007) 2376–2382.
[17] M.H. Cho, D.H. Ko, K. Jeong, S.W. Wang, C.N. Whang, S.C. Choi, S.J. Cho, Structural transition of crystalline Y_2O_3 film on Si(1 1 1) with substrate temperature, Thin Solid Films 349 (1999) 266–269.
[18] S.J. Park, D.P. Norton, Ion beam assisted texturing of polycrystalline Y_2O_3 films deposited via electron-beam evaporation, Thin Solid Films 510 (2006) 143–147.
[19] D. Basak, S.K. Sen, Electrical conduction in aluminium/yttrium oxide/aluminium sandwich structure, Phys. Stat. Sol. A 142 (1994) K37–K40.
[20] J.R.S. Havriliak, S. Negami, On the equivalence of dielectric and mechanical dispersions in some polymers, Polymers 10 (1969) 859–872.
[21] D.K. Davies, Charge generation on dielectric surfaces, Br. J. Appl. Phys. 2 (1969) 1549–1553.
[22] V.I. Arkhipov, J.A. Popova, A.I. Rudenko, Space-charge perturbed dispersive transport in disordered dielectrics, J. Electrostat. 18 (1986) 23–27.
[23] V.I. Arkhipov, A.I. Rudenko, D.V. Khramchenkov, Analysis of the Debye model of electret discharge, J. Electrostat. 25 (1990) 255–263.
[24] K. Kristiansen, A statistical approach to the analysis of dielectric breakdown strength of thin insulating films, Vacuum 27 (1977) 227–233.
[25] M. Mackey, A. Hiltner, E. Baer, L. Flandin, M.A. Wolak, J.S. Shirk, Enhanced breakdown strength of multilayered films fabricated by forced assembly microlayer coextrusion, J. Phys. D: Appl. Phys. 42 (2009) 1–12.
[26] P.M. Alt, D.B. Dove, W.E. Howard, Experimental results on the stability of AC thin-film electroluminescent devices, J. Appl. Phys. 53 (1982) 5186–5199.